Earth and Planetary Science Letters 311 (2011) 39–52

Contents lists available at SciVerse ScienceDirect

Earth and Planetary Science Letters

journal homepage: www.elsevier.com/locate/epsl

Post-depositional remanent magnetization lock-in for marine sediments deduced from ^{10}Be and paleomagnetic records through the Matuyama–Brunhes boundary

Yusuke Suganuma [a,*], Jun'ichi Okuno [a], David Heslop [b], Andrew P. Roberts [b], Toshitsugu Yamazaki [c], Yusuke Yokoyama [d]

[a] National Institute of Polar Research, 10-3 Midoricho, Tachikawa, Tokyo, 190-8518, Japan
[b] Research School of Earth Sciences, The Australian National University, Canberra, ACT 0200, Australia
[c] Geological Survey of Japan, AIST, 1-1-1 Higashi, Tsukuba, 305-8567, Japan
[d] Atmosphere and Ocean Research Institute, University of Tokyo, 5-1-5 Kashiwanoha, Kashiwa, 277-8568, Japan

ARTICLE INFO

Article history:
Received 18 January 2011
Received in revised form 20 August 2011
Accepted 26 August 2011
Available online 4 October 2011

Editor: P. DeMenocal

Keywords:
paleomagnetism
paleointensity
post-depositional remanent magnetization (PDRM)
lock-in depth
Matuyama–Brunhes boundary
^{10}Be

ABSTRACT

Geomagnetic field intensity records from marine sediments have contributed to improved understanding of variations in the Earth's magnetic field, and have helped to establish age models for marine sediments. However, lock-in of the geomagnetic signal below the sediment–water interface in marine sediments through acquisition of a post-depositional remanent magnetization (PDRM) adds uncertainty to synchronization of marine sedimentary records. Although quantitative models enable assessment of delays in remanence acquisition associated with PDRM processes, the nature of the filter function and the PDRM lock-in zone thickness remain topics of debate. We performed both forward numerical simulations and inverse parameter estimation to assess the best-fit filter function and PDRM lock-in zone thickness in marine sediments based on a comparison of ^{10}Be flux and relative paleointensity records. Our simulations reveal that the rate of PDRM lock-in increases in the middle of the lock-in zone and that a Gaussian function with a 17 cm lock-in zone thickness provides a good approximation to the PDRM lock-in within the studied core. With this function, PDRM lock-in is delayed, but with relatively little distortion of the geomagnetic signal. Our results also imply that a PDRM is not simply locked due to progressive marine sediment consolidation and dewatering, and that the arbitrary functions (linear, cubic, and exponential) that are often used to model PDRM lock-in starting from the base of the surface mixed layer cannot explain fully the observed paleomagnetic signal.

1. Introduction

Paleomagnetic studies of marine sediments have contributed to the development of age models based on magnetic reversal stratigraphy (e.g., Gradstein et al., 2004). Relative paleointensity records that span the last few thousands of years to the past few million years (e.g., Horng et al., 2003; Laj et al., 2000; Valet and Meynadier, 1993; Valet et al., 2005; Yamazaki and Oda, 2005) have also allowed development of high-resolution age models for sedimentary sequences (Inoue and Yamazaki, 2010; Kiefer et al., 2001; Macri et al., 2010; Mazaud et al., 2002; Stoner et al., 2000; Stott et al., 2002; Suganuma et al., 2009). Furthermore, because geomagnetic field intensity exerts an important control on cosmogenic radionuclide production rate, geomagnetic field intensity variability can also be used to synchronize marine sediments with ice cores by comparison of reconstructed ^{10}Be fluxes (Stoner et al., 2000). Cosmogenic radionuclides are therefore a powerful tool for synchronizing geological archives, which is essential for understanding changes in the Earth's climate system.

Despite its potential, geomagnetic synchronization has complications. It is widely considered that sediments become permanently magnetized through a post-depositional remanent magnetization (PDRM) mechanism (Irving and Major, 1964; Kent, 1973). Immobilization of magnetic particles is thought to occur during sediment dewatering and compaction, which causes vertical offsets between the sediment/water interface and the zone where the paleomagnetic record is fixed (Verosub, 1977). This offset is called the PDRM lock-in depth, and the magnitude of this depth has long been debated (e.g., Channell and Guyodo, 2004; deMenocal et al., 1990; Knudsen et al., 2008; Liu et al., 2008; Roberts and Winklhofer, 2004; Sagnotti et al., 2005; Tauxe and Yamazaki, 2007; Tauxe et al., 1996, 2006). Suganuma et al. (2010) estimated the PDRM lock-in depth for marine sediments based on an offset between high-resolution ^{10}Be flux and paleomagnetic records through the Matuyama–Brunhes (M–B) boundary. Although they demonstrated that acquisition of the paleomagnetic record is delayed relative to the ^{10}Be record, details of the remanence acquisition mechanism remain unclear.

* Corresponding author. Tel.: +81 42 512 0702.
E-mail addresses: suganuma.yusuke@nipr.ac.jp (Y. Suganuma), okuno@nipr.ac.jp (J.' Okuno), david.heslop@anu.edu.au (D. Heslop), andrew.roberts@anu.edu.au (A.P. Roberts), toshi-yamazaki@aist.go.jp (T. Yamazaki), yokoyama@aori.u-tokyo.ac.jp (Y. Yokoyama).

0012-821X/$ – see front matter © 2011 Elsevier B.V. All rights reserved.
doi:10.1016/j.epsl.2011.08.038

PDRM acquisition in marine sediments has been analyzed in numerical model studies (e.g., Bleil and von Dobeneck, 1999; Channell and Guyodo, 2004; Hyodo, 1984; Kent and Schneider, 1995; Meynadier and Valet, 1996; Roberts and Winklhofer, 2004). These approaches suggest that some filtering process acts during PDRM lock-in to modify the input geomagnetic signal. However, the form of the filter function and the thickness of the PDRM lock-in zone remain topics of debate. ^{10}Be flux records in marine sediments provide complementary information to relative paleointensity records for assessing past geomagnetic field intensity variations. This makes it possible to assess the PDRM filter function by comparing ^{10}Be flux and relative paleointensity records from marine sediments, with the caveat that the ^{10}Be flux record is also "filtered" by surface mixing due to bioturbation. However, using ^{10}Be flux and relative paleointensity records from the same sedimentary sequence can allow discrimination between the effects of surface mixing and PDRM filtering processes in marine sediments.

We present forward model results with several different lock-in functions to assess the best-fit function and PDRM "lock-in zone" thickness in marine sediments. We also determine empirically a PDRM lock-in function using an inverse estimation based on obtaining the best possible match between a deconvolved ^{10}Be flux record and the measured relative paleointensity record. Our approach provides important insights into understanding sedimentary PDRM lock-in.

2. Material and microtektite analysis

The studied piston core MD982187 was recovered from a water depth of ca 4600 m in the western equatorial Pacific Ocean (4.27° N, 134.82° E). Discrete cubic paleomagnetic samples (7 cm^3) were collected from split half cores. Detailed paleomagnetic and ^{10}Be results are described by Yamazaki and Oda (2005) and Suganuma et al. (2010), respectively.

Microtektite analysis was carried out to detect the thickness of the sedimentary surface mixed layer, following the method of Schneider et al. (1992). The sediment samples were treated with 0.1 M HCl, a 20% solution of H_2O_2, and 5% sodium hexametaphosphate to remove carbonate and residual organics, and to aid disaggregation. The samples were wet-sieved and the >125 μm fraction was visually searched for microtektites using a binocular microscope. We counted both microtektites and microtektite fragments, which could be identified based on their characteristic shapes and glassy appearance under reflected light (Table A.1, Fig. A.1).

3. Thickness of the lock-in zone and surface mixed layer

^{10}Be flux and paleomagnetic records are expected to have different characteristic functions that represent the manner in which the

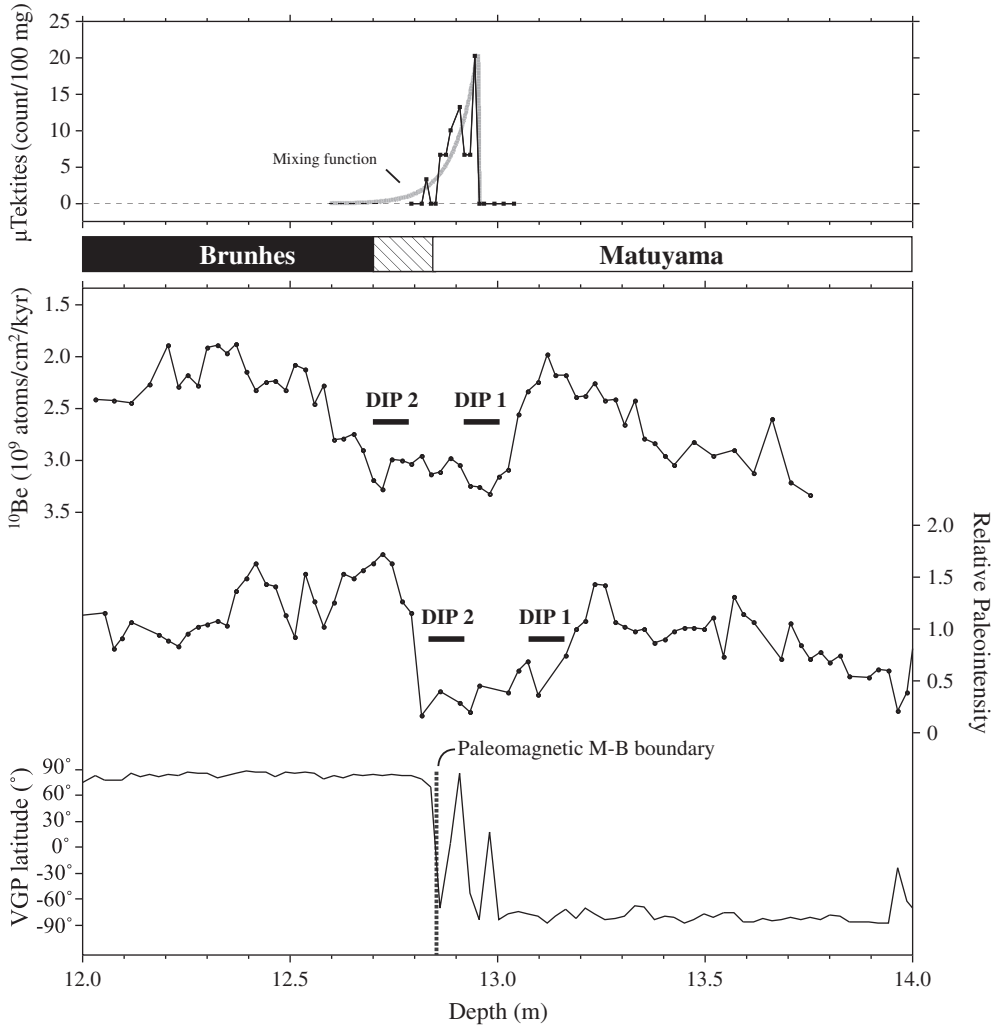

Fig. 1. Microtektite concentration, ^{10}Be flux, relative paleointensity, and virtual geomagnetic pole (VGP) latitude for core MD982187. M–B: Matuyama–Brunhes boundary. DIP1 and DIP2 correspond to paleointensity minima at the 'precursor' event and M–B boundary, respectively (cf. Hartl and Tauxe, 1996). A mixing function for ^{10}Be flux is estimated from the microtektite dispersion (gray curve, upper panel).

geomagnetic signal was locked-in. The ^{10}Be flux record is thought to be fixed through a surface mixing process, associated with bioturbation. To evaluate the surface mixed layer thickness, microtektite analysis was carried out for core MD982187. A peak in microtektite concentration occurs at 12.95 m, just below the M–B boundary (Fig. 1, Table A.1). Microtektite deposition is geologically instantaneous, therefore the stratigraphically dispersed microtektite horizon observed in core MD982187 can be attributed to the mixing action of bioturbation. Based on the observed microtektite concentrations as a function of depth, the biological sediment mixing function can be estimated using a time-dependent eddy diffusion model (Guinasso and Schink, 1975). The sediment mixing function should thus represent the thickness of the "lock-in" zone for the ^{10}Be flux record and was estimated using the approximate analytical procedures outlined by Officer and Lynch (1983) (Fig. 1). This estimation indicates that 95% of the mixing took place within a 17-cm sediment thickness. For comparison an estimated global average thickness of the surface mixed layer is 9.8 cm (Boudreau, 1994; 1998). ^{10}Be-bearing particles will have been mixed by bioturbation to the same extent as other paleoclimatic proxies, such as planktonic foraminiferal δ^{18}O records. Thus, ^{10}Be and paleomagnetic signals will be displaced downward by bioturbation, but any additional depth offset between the ^{10}Be flux and relative paleointensity records is attributable to delayed PDRM lock-in relative to the ^{10}Be record.

The relative paleointensity record through the M–B boundary from core MD982187 (Fig. 1) contains two clear minima around the M–B boundary, which indicates that the geomagnetic field was weak, as expected, during the polarity transition (e.g., Valet et al., 2005). In terms of a switch in polarity, the M–B boundary occurs at the mid-point of the uppermost paleointensity minimum (DIP2). The preceding small minimum is believed to be a manifestation of the 'precursor' event (DIP1), which occurred between ca 10 and 17 kyr before the M–B boundary (e.g., Hartl and Tauxe, 1996; Kent and Schneider, 1995; Macri et al., 2010; Singer et al., 2005). The ^{10}Be flux record also has similar long-term variations, but a clear offset is present between the large-scale first-order variations in ^{10}Be flux and relative paleointensity. The ^{10}Be flux and paleomagnetic records are from the same marine sedimentary core, therefore depth offsets between the records can be attributed to delays resulting from PDRM lock-in. To evaluate depth offsets, correlation coefficients between the ^{10}Be flux and relative paleointensity records were calculated at corresponding depths for different offsets between the records (Fig. 2). Based on the highest correlation coefficient between the two records, the PDRM lock-in depth in this core is estimated to be ca 16 cm. Importantly, even smaller-scale ^{10}Be flux and relative paleointensity variations appear to be correlated with each other, with both records containing marked double minima (DIP1 and DIP2) (corresponding to ^{10}Be maxima).

4. Forward modeling: best fit lock-in model for PDRM and ^{10}Be flux

Quantitative models of PDRM lock-in processes have used several types of parametric lock-in function. The most commonly used function is an exponential type (e.g., Hamano, 1980; Hyodo, 1984; Kent and Schneider, 1995; Meynadier and Valet, 1996; Otofuji and Sasajima, 1981). PDRM is assumed to become locked as a result of progressive sediment consolidation and dewatering (e.g., Irving and Major, 1964; Kent, 1973). These processes gradually reduce interstitial voids in sediments, so that sediment particles can no longer be rotated by the torque exerted by the

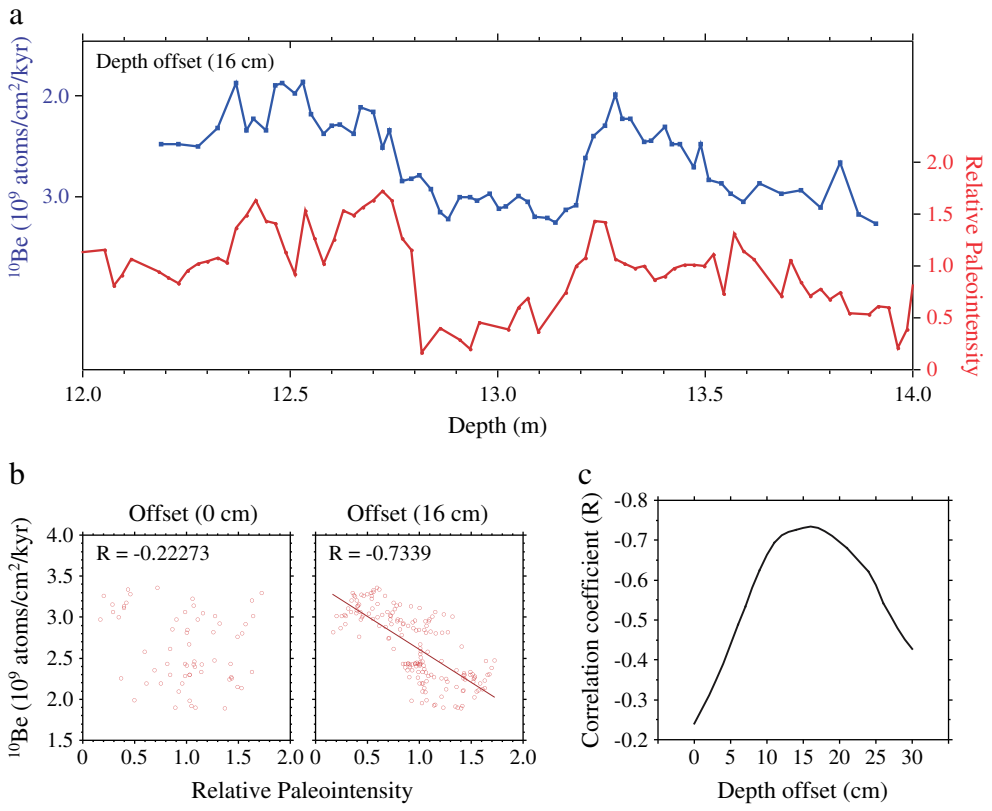

Fig. 2. Depth offset estimation based on correlation coefficients between the ^{10}Be flux and relative paleointensity records. The ^{10}Be flux record was displaced by different amounts from 0 to 30 cm to find the best-fit depth offset based on the best correlation coefficient. With no depth offset the correlation is low, but reaches a maximum for a depth offset of 16 cm (and is significant at the $P \leq 0.001$ level; note that this significance level does not consider reduction in the number of degrees of freedom due to autocorrelation).

geomagnetic field. Sediment consolidation often proceeds in an exponential manner during its initial stages (Lambe and Whitman, 1969) so that an exponential function is considered reasonable for representing the PDRM lock-in process (Roberts and Winklhofer, 2004). Other types of functions have also been used to model PDRM lock-in, such as linear and cubic functions (Bleil and von Dobeneck, 1999; Roberts and Winklhofer, 2004). The actual mechanisms controlling PDRM lock-in remain unknown, so it is reasonable to consider a range of functions to quantitatively model PDRM acquisition (Fig. 3a). We include a Gaussian lock-in function (Fig. 3a) with which the geomagnetic signal is mostly fixed within a narrow depth interval located within the center of the lock-in zone. The PDRM lock-in process expressed by this function therefore cannot be simply explained by progressive sediment consolidation and dewatering in the uppermost sediment column.

The stratigraphic dispersion of microtektites makes it possible to estimate the surface mixed layer thickness and the form of the "lock-in function" for the ^{10}Be flux record. Based on the observed microtektite dispersion, the time-dependent eddy diffusion mixing function obtained above was employed to represent bioturbation in the forward model (Fig. 3b). Although ^{14}C dates from the surface mixed layer in marine sediments often appear to be constant (Thomson et al., 2000), the microtektite distribution suggests that surface mixing in MD982187 can be represented by this function, which provides an estimate of the filter to which the ^{10}Be record has been subjected, and enables comparison with the PDRM lock-in process.

We assume that the PDRM lock-in process depends on burial depth in marine sediments rather than burial time because the fixing of magnetic grains in sediments is thought to be mainly caused by progressive sediment consolidation and dewatering. A high-resolution paleomagnetic record from Ocean Drilling Program (ODP) Site 983 (Channell and Kleiven, 2000) was transferred onto an artificial depth scale, based on the average sedimentation rate of the Brunhes Chron (1.65 cm) for core MD982187, to provide an input geomagnetic signal in our model (Fig. 4). A ^{10}Be flux was then simulated from the input Site 983 geomagnetic data based on the global production rate for ^{10}Be particles as a function of field intensity given by Wagner et al. (2000). Although the double dip structure of the ODP Site 983 record of Channell and Kleiven (2000) is not as clear as in the ^{10}Be and relative paleointensity records of core MD982187, we still recognize a small dip that corresponds to precursor DIP1 in addition to the main DIP2 at the M–B boundary. The geomagnetic polarity change in our model is simulated by a simplified version of the changes in the virtual geomagnetic pole (VGP) latitude of the ODP Site 983 record. The input signal reflects the nearly instantaneous switch in VGP latitude corresponding to the M–B boundary in the record with a subsequent rapid reversal in polarity (Fig. 4). While the high-resolution relative paleointensity record from ODP Site 983 has been filtered by PDRM processes, the sedimentation rate for this core was approximately 10 times higher than for core MD982187. We therefore assume that the resolution of the ODP Site 983 paleointensity record is adequate to treat it as a representative input for geomagnetic field intensity variations.

Our procedure for modeling PDRM lock-in processes is as follows. The fraction of the locked magnetic moment can be described by linear, exponential, cubic and Gaussian (Fig. 3a) lock-in functions $FL(z)$, which depend on depth (z). The lock-in function $FL(z)$ describes the relative contribution of each layer z' to the total PDRM acquired at z, down to a depth λ (where $\lambda = \delta + F$, Fig. 3) below the sediment/water interface such that:

$$PDRM(z) = \int_0^{\lambda} B(z-z')FL(z')dz', \quad (1)$$

where $B(z)$ is the input geomagnetic time series from ODP Site 983 (Channell and Kleiven, 2000). For numerical modeling, it is suitable to transform the depth domain into a regular grid, $B(z)$ to $B(j)$. In addition, the surface mixed layer produces a constant offset δ, which can be represented by a constant D. Thus, the PDRM lock-in can be calculated by convolving the geomagnetic input signal with the respective lock-in filter function:

$$PDRM(j) = \sum_{k=0}^{L-D} B(j-k)FL(k), \quad (2)$$

where L is the lock-in depth in the discrete coordinate system. The model will represent the recorded paleomagnetic signal after PDRM lock-in filtering of the geomagnetic input signal. Calculations of PDRM lock-in were made at 0.1 cm stratigraphic intervals (sediment compaction resulting from burial is not considered in our model).

Paleointensity variations were calculated using all of the lock-in functions shown in Fig. 3a with different lock-in zone thicknesses. These calculations are compared with the calculated ^{10}Be flux to find the best-fit lock-in filter function and to estimate the PDRM lock-in depth for these marine sediments (Fig. 5a, b). Our calculations are performed for the short sequence containing the M–B boundary because the ^{10}Be flux record for core MD982187 was only obtained from this interval (Suganuma et al., 2010). We have also offset our calculated paleointensity record by 16 cm relative to the ^{10}Be flux

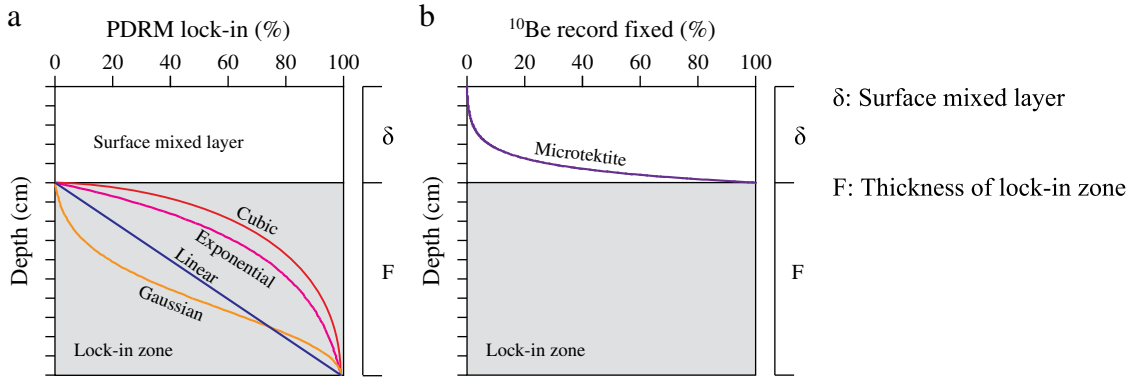

Fig. 3. Schematic illustrations of lock-in functions for a PDRM and ^{10}Be flux. (a) Cumulative percentage of PDRM lock-in with depth for linear, exponential, cubic, and Gaussian functions. PDRM lock-in for all functions ceases at 99%. (b) Time-dependent eddy diffusion model fit to the microtektite distribution that is used to represent the mixing function of the ^{10}Be flux record due to surface bioturbation. The surface mixed layer is considered to shift the paleomagnetic signal downward without filtering, therefore it is reasonable to treat PDRM lock-in as commencing after substantial bioturbation ceases.

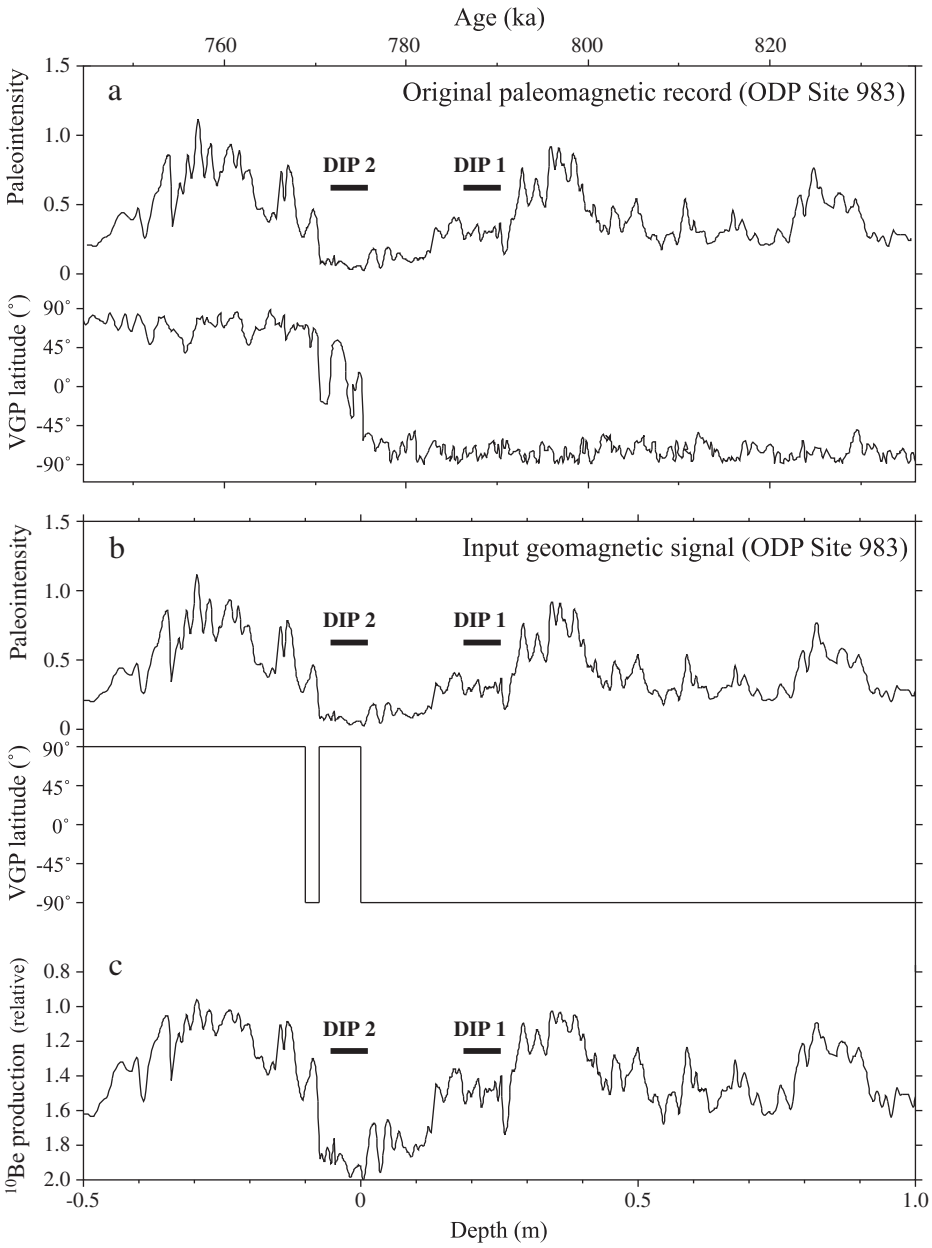

Fig. 4. Paleointensities, VGP latitudes, and ^{10}Be flux record employed as the input geomagnetic signal for forward modeling of PDRM lock-in. (a) The paleomagnetic record, including relative paleointensity and virtual geomagnetic pole (VGP) latitude, is from ODP Site 983 (Channell and Kleiven, 2000). (b) The input geomagnetic signal is transferred from the original paleomagnetic record onto an artificial depth scale based on the average sedimentation rate of the Brunhes Chron (1.65 cm) for core MD982187. The geomagnetic polarity change at the M–B boundary is simulated using a series of instantaneous 180° flips in VGP latitude to mimic the ODP Site 983 record. A depth of 0 m is assigned to the M–B boundary, and polarity switches are set at −10 cm and −7.5 cm (as defined by the VGP latitude changes). (c) ^{10}Be flux record calculated using the relative paleointensity record in (b) based on the relationship for ^{10}Be production as a function of geomagnetic field intensity from Wagner et al. (2000).

record to adjust for the depth difference in the original position of the M–B boundary between these records (Fig. 2c).

The ^{10}Be flux was calculated using a lock-in function deduced from the microtektite dispersion to represent the surface mixing process. The calculated ^{10}Be flux is compared with the ^{10}Be flux record for core MD982187 in Fig. 6a. These curves have similar long-term variations and patterns with double minima that correspond to DIP1 and DIP2, although small discrepancies exist. This indicates that the model calculations could reproduce the filtering process for the ^{10}Be record associated with surface mixing. On the other hand, paleointensity calculations produce variable levels of reproducibility that depend on the thickness of the lock-in zones for different filter functions (Fig. 5a, b). For lock-in zone thicknesses of 5 cm, 10 cm, and 25 cm, none of the simulated paleointensity curves for any of the functions fit the calculated ^{10}Be flux record in terms of the positions of maxima and minima (Fig. 5a). This indicates that such lock-in zones are either too thin or too thick. In contrast, lock-in zone thicknesses between 15 and 21 cm provide similar paleointensity curves compared to those calculated from ^{10}Be fluxes (Fig. 5b). However, as expected, high-frequency characteristics decrease with thicker lock-in zones, especially for linear, exponential, and cubic functions. To evaluate similarities among the model results, we calculated correlation coefficients between the simulated ^{10}Be and paleointensity records (Table 1). The paleointensity curves for exponential and cubic functions have the highest correlation coefficient for a lock-in depth of 21 cm. Linear and Gaussian functions have the

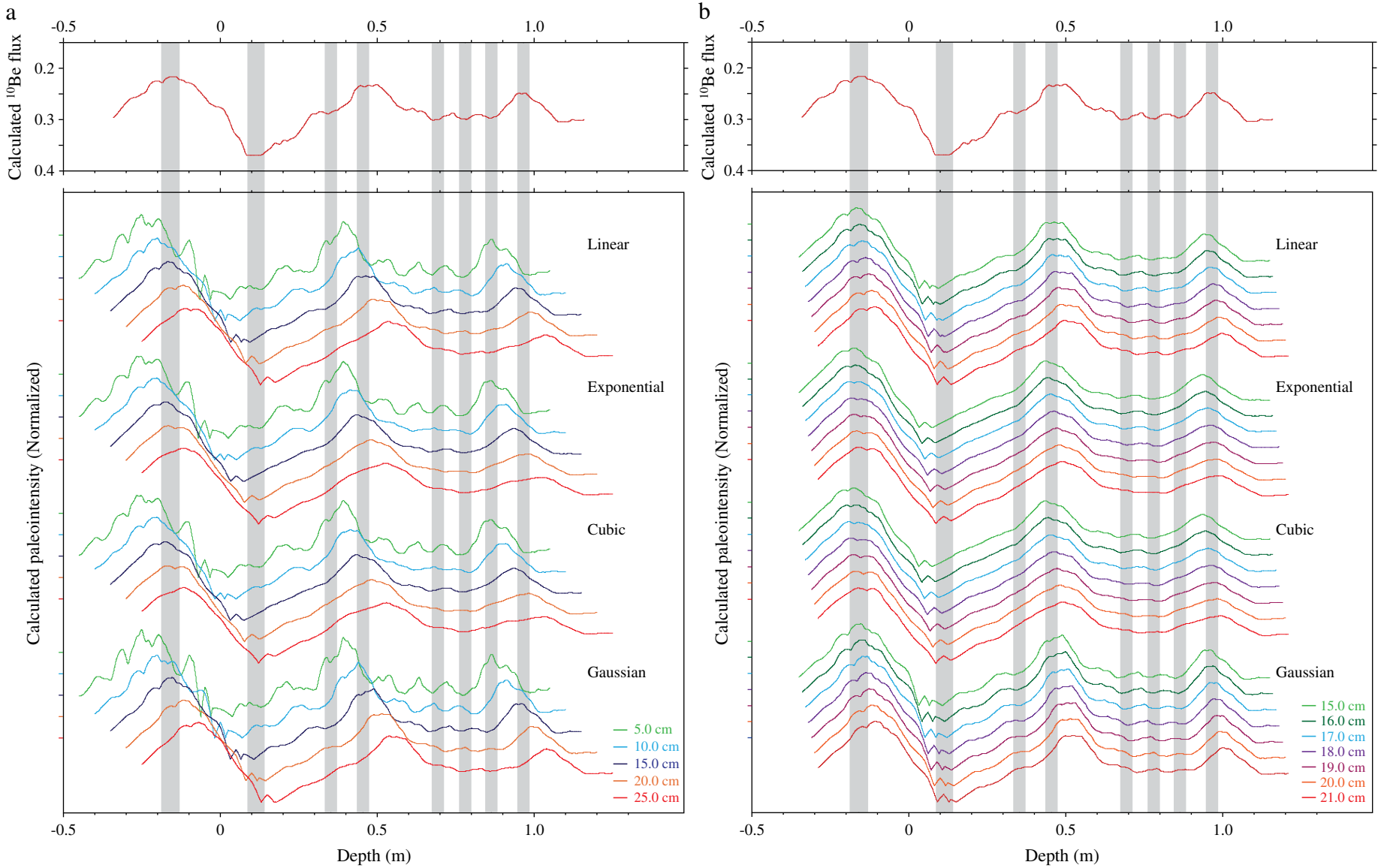

Fig. 5. Paleointensity records calculated using linear, exponential, cubic, and Gaussian functions for lock-in zones with *F* values of (a) 5, 10, 15, 20, and 25 cm, and (b) 15, 16, 17, 18, 19, 20, and 21 cm. Upper panel: ^{10}Be flux calculated using a mixing function to account for bioturbation. The gray shaded intervals mark maxima and minima in the ^{10}Be flux.

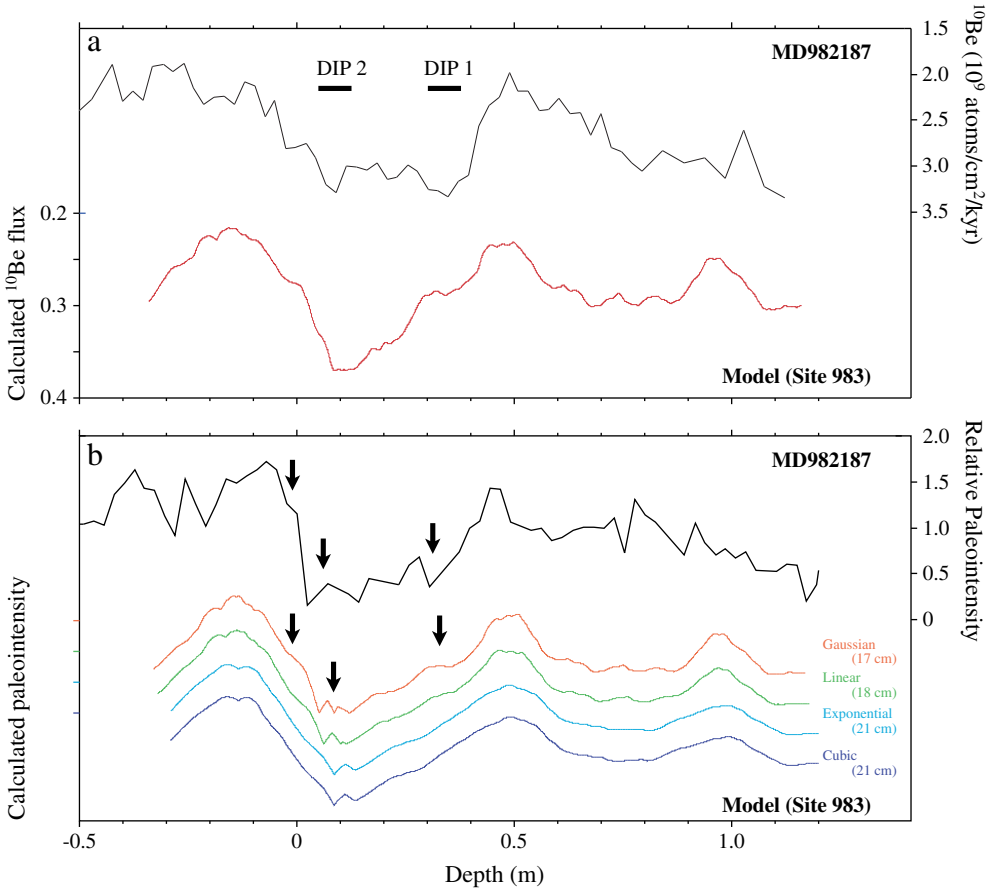

Fig. 6. Results of forward lock-in model calculations for paleointensity and ^{10}Be flux records for the highest respective correlation coefficients for different filter functions. (a) ^{10}Be flux for core MD982187 compared to a model calculation for the ODP Site 983 paleointensity record (Channell and Kleiven, 2000) using a mixing function to represent bioturbation and a sedimentation rate of 1.65 cm/kyr for core MD982187. (b) Paleointensity records from core MD982187 and model calculations using linear, exponential, cubic, and Gaussian functions with lock-in depths that yield the highest correlation between the respective records. Black arrows denote high-frequency features.

highest correlation for lock-in thicknesses of 18 cm and 17 cm, respectively. To discuss characteristics of the lock-in process for each function, we compare model outputs at the highest correlation coefficient with the paleointensity record for core MD982187 (Fig. 6b). These curves generally have similar long-term patterns. However, the details are slightly different for each function. For example, the paleointensity curve for a Gaussian lock-in function has a small minimum that corresponds to the M–B precursor (DIP1), whereas the dip is not recognized with the other filter functions. Likewise, the Gaussian filter function produces a sharper peak at the paleointensity maximum 0.3 m below the M–B boundary. In order to compare the finer detail of each function, we carried out a high-pass filter analysis (Fig. A.2). The high-pass filtered data of the Gaussian function has the highest correlation coefficient with the simulated ^{10}Be record for Site 983. These observations suggest that a Gaussian lock-in function is more suitable than the other functions for preserving high-frequency characteristics of the input geomagnetic signal. The paleointensity and ^{10}Be records for core MD982187 also clearly contain DIP1, therefore optimal lock-in models should also reproduce the high-frequency characteristics of the geomagnetic signal that appear to be consistent between paleointensity records.

The effect of simplifying the changes in VGP latitude during the M–B boundary (Fig. 4) is tested using an alternative input signal. The geomagnetic polarity in this alternative model is simplified to a single instantaneous switch in the VGP latitude (Fig. A.3). Based on this input signal, paleointensity variations were calculated using all of the lock-in functions with different lock-in zone thicknesses, and compared with the calculated ^{10}Be flux (Fig. A.4a, b). The resulting models have similar variations and patterns to the complex VGP model (Fig. 5a, b), although a small wiggle is no longer observed at DIP2. In addition, the thickness of the best-fit function is slightly smaller than in the original model (Table A.2). These differences are caused by the short polarity event in the complex VGP model (Fig. 4), however, this appears to influence only minor details of DIP2. This indicates that preservation of high-frequency characteristics of the input geomagnetic signal throughout the data is not changed significantly between the models. Thus, we prefer to retain the more realistic geomagnetic signal (complex VGP model) in the forward model.

Table 1
Correlation coefficients between simulated paleointensity and ^{10}Be flux records for different lock-in zone thicknesses.

Thickness of lock-in zone	Function			
	Linear	Exponential	Cubic	Gaussian
5	0.514	0.482	0.478	0.537
10	0.749	0.693	0.691	0.783
15	0.937	0.889	0.888	0.955
16	0.959	0.917	0.916	0.970
17	0.970	0.938	0.937	**0.972**
18	**0.973**	0.952	0.950	0.964
19	0.969	0.961	0.960	0.949
20	0.961	0.967	0.965	0.928
21	0.948	**0.968**	**0.967**	0.902
25	0.855	0.941	0.941	0.753

Bold indicates optimal correlation.

5. Inverse modeling: PDRM lock-in function estimated from the ^{10}Be flux record

In addition to assessing the suitability of different PDRM lock-in functions using forward modeling, we have attempted inverse modeling to estimate directly the best-fit filter function through inversion of the MD982197 ^{10}Be flux record. The inverse estimation procedure requires three steps. First, the effects of bioturbation must be removed from the MD982187 ^{10}Be flux record to provide an estimated pristine record of ^{10}Be flux. Second, the estimated pristine ^{10}Be flux record must be modified to provide a representation of field intensity that includes sign changes at the M–B boundary. Finally, it is necessary to find the lock-in function that, when convolved with the ^{10}Be-based geomagnetic intensity record, yields the best possible match to the measured MD982187 relative paleointensity record.

To recover an undisturbed record of ^{10}Be flux and hence an estimate of past geomagnetic field intensity, deconvolution was performed on the ^{10}Be flux record obtained from core MD982187. A triangular function representing bioturbation in the surface mixed layer was constructed based on the model fitted to the distribution of microtektites shown in Fig. 1 (constructed with one point per centimeter and normalized to a sum of 1 to ensure conservative mixing). Deconvolution by spectral division (Aster et al., 2005) of the sedimentary ^{10}Be flux record (interpolated onto an equally spaced depth scale at 1 cm intervals) by the bioturbation function was performed to estimate the undisturbed ^{10}Be flux.

In an attempt to limit introduction of artificial noise during deconvolution, a water level regularization scheme was adopted to prevent amplification at frequencies where the spectral amplitude of the bioturbation function is small (Aster et al., 2005). Water level regularization employs a threshold parameter, ω, with which small spectral amplitudes can be adjusted to produce a more stable deconvolved signal (as ω increases, the deconvolved signal will become smoother, but high values of ω will produce too much smoothing). It is a challenge to find the optimal value of ω; however, its value can be constrained through application of physically realistic assumptions. Assuming that bioturbation will smooth the recorded ^{10}Be flux, the variance of the deconvolved record must be greater than or equal to that of the sedimentary record, thus providing an upper limit on ω. The ratio of the variance of the deconvolved and sedimentary ^{10}Be records as a function of ω for surface mixed layer thicknesses between 9 and 13 cm is shown in Fig. A.5. For these thicknesses, the upper limit of ω lies in the interval [0.36, 0.56]. An example of the deconvolved ^{10}Be record for a surface mixed layer thickness of 11 cm and $\omega = 0.3$ is shown in Fig. 7a.

Once a suitably deconvolved record of ^{10}Be flux is obtained it can provide a representation of the geomagnetic field intensity by assuming that the square-root dipole field intensity is approximately inversely proportional to the global production of ^{10}Be (Lal and Peters, 1967). However, the proportionality coefficient of this approximation is unknown. Representation of the field intensity depth series can therefore only be considered in terms of its shape rather than its absolute values. In the paleomagnetic record, the M-B boundary is positioned within the DIP2 paleointensity minimum (Fig. 1). To represent the change in sign of the field at the M–B boundary, the depth 12.64 m (corresponding to the minimum in DIP2 in the deconvolved ^{10}Be record, Fig. 7a) was selected as the point at which the field reversed polarity between VGPs of −90° and 90°. To represent this polarity flip, a constant was subtracted from the depth series so that the value at 12.64 m equaled zero. All points below 12.64 m were then multiplied by −1 to represent reversed polarity fields. Finally, the modified depth series was normalized to have unit variance (Fig. 7b).

An empirical lock-in function for the MD982187 sediments through the M–B boundary was determined by estimating the function that when convolved with the calculated field intensity record would provide an optimal representation of the sedimentary paleointensity record (interpolated onto the same 1 cm depth intervals). To find the lock-in function, a matrix consisting of lagged versions of the ^{10}Be-based field intensity depth series was constructed. The first column represented the first point below the surface mixed layer (assumed to be 11 cm thick), with each subsequent column containing a version of the depth series offset by 1 cm, up to a predefined maximum lock-in depth. A lock-in function is then given by n non-negative coefficients (where n is the number of columns in the prepared matrix) that when matrix multiplied with the prepared matrix will produce a depth series that represents the convolution of the ^{10}Be-based field intensity and the lock-in function. To provide a meaningful comparison with the relative paleointensity record only the magnitudes of the convolved depth series can be considered (because paleointensity cannot take negative values). It is therefore necessary to find the lock-in function that yields a convolved depth series with absolute values that provide the best match to the relative

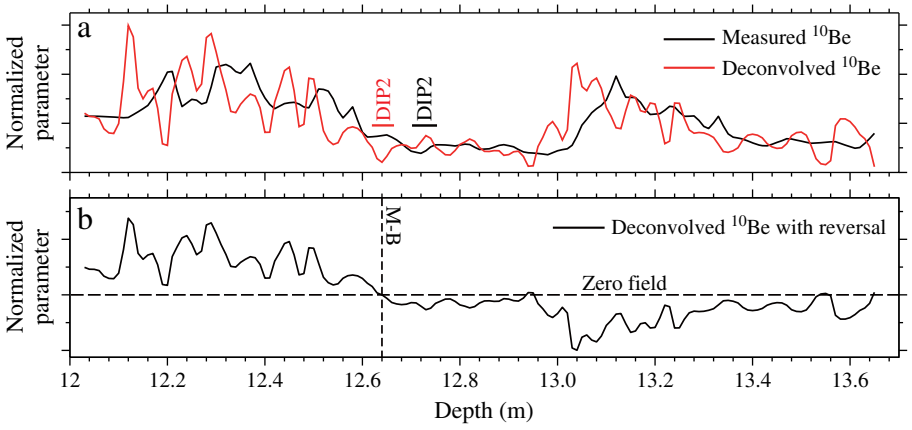

Fig. 7. (a) Example ^{10}Be flux record (red line) obtained by deconvolution ($\omega = 0.3$) of the sedimentary ^{10}Be flux record (black line) with a triangular function designed to represent bioturbation. The surface mixed layer was assumed to have a thickness of 11 cm. In this case the variance of the deconvolved signal is ~20% higher than the input sedimentary record. The positions of DIP2 in the measured and deconvolved records are shown. As expected the intensity minimum is ~11 cm shallower after the effects of biological mixing are removed. (b) To represent the polarity switch at the M–B boundary the geomagnetic field strength at the minimum of DIP2 in the deconvolved ^{10}Be flux record (dashed vertical line) was assumed to be zero (dashed horizontal line) and all points below this depth were multiplied by −1.

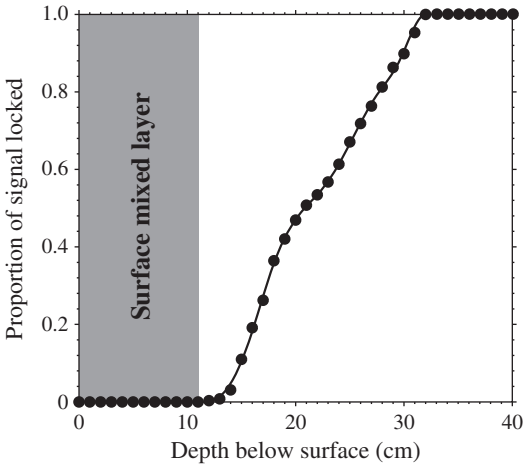

Fig. 8. The estimated PDRM lock-in filter function obtained from inversion of the ^{10}Be flux record. The function is monotonic due to the imposed non-negativity constraints and indicates that the PDRM lock-in begins at ~14 cm and effectively ceases at ~32 cm (the surface mixed layer is assumed to have 11 cm thickness and $\omega = 0.3$). Thus, the inverse modeling procedure yields a lock-in zone thickness of ~21 cm.

paleointensity data, which was assessed by maximizing the Pearson product-moment correlation coefficient (r). The lock-in function coefficients were found using a derivative-free optimization algorithm (Nelder–Mead simplex method) that was employed to maximize r with a non-negativity constraint placed on each coefficient (Lagarias et al., 1998).

To determine an appropriate width for the lock-in function, the optimization procedure described above was performed at increasing depth intervals up to 40 cm. At each thickness the value of r at which the optimization algorithm converged was recorded and converted into an adjusted coefficient of multiple determination (R^2_p), which accounts for the numbers of degrees of freedom in the fit (Swan and Sandilands, 1995). Thus, R^2_p should increase with the width of the lock-in function (because more variables will improve the model fit), until improvement in the fit is insufficient to compensate for the addition of a degree of freedom each time the lock-in function thickness is increased by 1 cm. Therefore, the most appropriate width for the lock-in function was selected when R^2_p was maximized, in this case at a thickness of 32 cm (Fig. A.6).

The cumulative sum of the lock-in coefficients (normalized to unit sum), which when convolved with the ^{10}Be-based field intensity depth series, yields the best-fit representation of the relative paleointensity (in this case constructed assuming a surface mixed layer thickness of 11 cm, a total lock-in thickness of 32 cm and with $\omega = 0.3$) is shown in Fig. 8. The large-scale structure of the estimated lock-in function illustrates that PDRM lock-in commences slowly just below the surface mixed layer and then accelerates to a relatively constant rate of acquisition. The depth series produced by the convolution of the ^{10}Be-based field intensity with the lock-in coefficients is shown in Fig. 9a. The two depth series correlate for the large-scale structure of the paleointensity minimum associated with the reversal ($r = 0.78$ over the full length of the records), however, there is poor correspondence for second-order variations. Normal and reversed polarity contributions to the modeled depth series are shown in Fig. 9b.

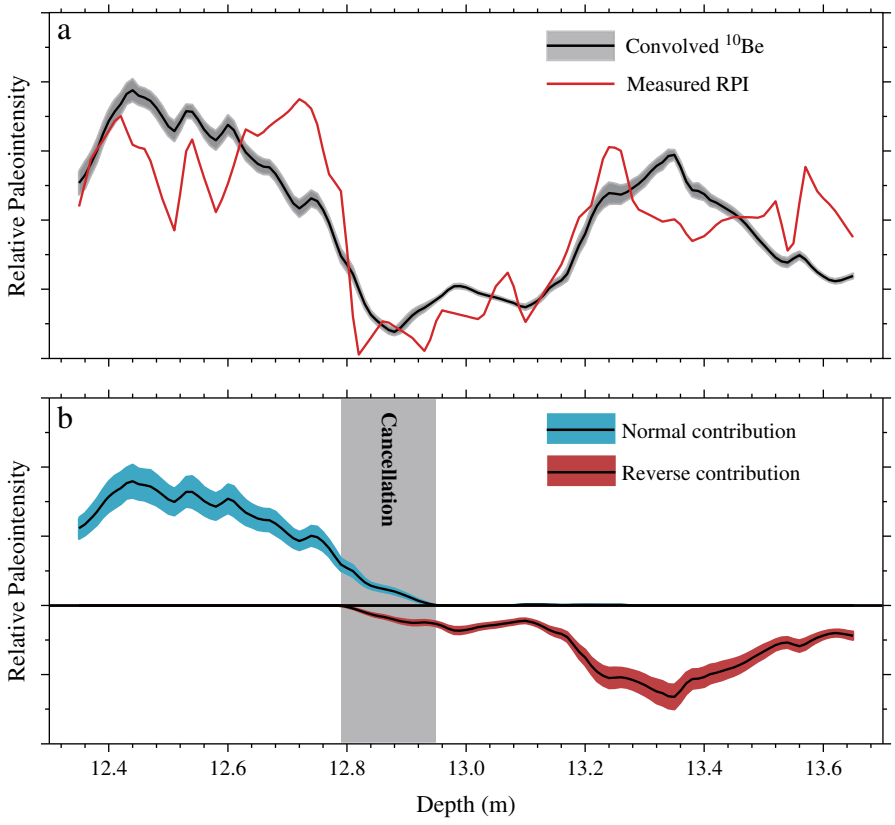

Fig. 9. (a) Comparison between the measured RPI depth series (red line) and the deconvolved ^{10}Be flux convolved with the optimal lock-in function (black line, with shading representing the standard deviation of the depth series estimated from 100 runs of the optimization algorithm with different initializations). (b) The normal and reversed polarity contributions to the overall convolved depth series shown in (a). Shading represents the standard deviation. The region with partial cancelation of normal and reversed polarity contributions (gray zone) is relatively narrow and does not have a strong effect on the final record.

Cancelation of the normal and reversed components is limited to a narrow window around DIP2 (i.e., the M–B boundary) and does not have a strong influence on the final record because the field strength in this region is close to zero. If the M–B polarity reversal was longer than assumed in the model, then the width of the cancelation zone would be expected to increase. Alternatively, if a more complex VGP pattern was used to represent the reversal the effects of cancelation could increase. Numerical experiments of this type suggest, however, that the influence of a more complex VGP path on the final intensity curve is limited because fields through the transition zone are close to zero.

6. Discussion

Our forward model results suggest that, from the collection of examined functions, a Gaussian function is the most suitable lock-in function for preserving high-frequency characteristics of the input geomagnetic signal. Roberts and Winklhofer (2004) reported that the paleomagnetic record is drastically smoothed even for sediments with a lock-in depth of 10 cm (where 95% of the PDRM is locked within 5 cm of the base of the surface mixed layer) in the case of cubic, linear and exponential functions. Our results further demonstrate that linear, exponential, and cubic functions considerably smooth the original geomagnetic signal. We have assumed that the PDRM starts to lock-in just after substantial bioturbation ceases, and that surface mixing simply shifts the paleomagnetic signal downward without filtering. Alternatively, if PDRM lock-in starts before substantial bioturbation ceases (cf. Channell and Guyodo, 2004), these functions will cause even greater smoothing. The empirical PDRM lock-in function estimated using an inverse modeling approach suggests that PDRM lock-in starts slowly below the base of the surface mixed layer and intensifies in the deeper parts of the lock-in zone, contrary to expectation from commonly used PDRM lock-in functions (linear, cubic, and exponential). This phenomenon likely explains why PDRM lock-in within core MD982187 is delayed, but with relatively weak filtering of the geomagnetic signal.

PDRM lock-in is commonly thought to result from progressive sediment consolidation and dewatering. The water content of marine sediments from the central and western equatorial Pacific Ocean is reported to start decreasing just below the sediment–water interface down to depths of 10–15 cm (Ikehara and Nishimura, 1993; Ikehara et al., 1992; Yamazaki, 1992). This suggests that significant sedimentary dewatering ceases before much of the PDRM is locked. Our observations suggest that the PDRM is not simply locked as a result of progressive consolidation and dewatering of marine sediments, and that commonly used lock-in functions for PDRM modeling that start to produce lock-in from the base of the surface mixed layer (linear, cubic, and exponential) cannot explain the observed paleomagnetic signal in core MD982187. Accordingly, initiation of PDRM lock-in is not simply shifted downward by surface mixing in sediments. Channell and Guyodo (2004) documented a large paleomagnetic offset due to PDRM lock-in, but with relatively weak filtering. Although they proposed a thick surface mixed layer overlying a thin PDRM lock-in zone to explain this phenomenon, our interpretations can probably also explain their observations with a thicker lock-in zone and a thinner overlying mixed layer.

Sediment particles remain free to mechanically rotate (depending on particle flocculation; Tauxe et al., 2006) at higher water contents, and become locked as dewatering proceeds. The range of water contents at which particle locking occurs is probably lower than the significant dewatering observed down to 15 cm in marine sediments (Ikehara and Nishimura, 1993; Ikehara et al., 1992; Yamazaki, 1992). Carter-Stiglitz et al. (2006) reported that the efficiency of detrital remanent magnetization (DRM) acquisition is strongly dependent on water content based on redeposition experiments using a dilute solution of gelatin, which gels below 20 °C. DRM efficiency was reduced nearly to zero when the water content fell below 50% in their sample material (sediments from ODP Site 851). Importantly, they argued for a certain water content range for PDRM lock-in as constrained from an original NRM/ARM value for the core. Although they concluded that the upper limit of the water content range is controlled by bioturbation, the specific range of water contents possibly corresponds to the fixing zone of sediment particles. This suggests that particles remain free to physically rotate at higher water contents, which may explain the PDRM lock-in zone observed here. However, the critical range of water contents will almost certainly depend on the lithology of the sediments under consideration.

Chemical or bio-chemical effects can exert additional influences on the PDRM lock-in zone. The extent of sediment flocculation is controlled by salinity and pH (Katari and Tauxe, 2000; Tauxe et al., 2006). Thus, if chemical or bio-chemical processes change the pore water chemistry, it may be possible for different floc sizes to reorient variably within the geomagnetic field. Unfortunately, we do not have further data to elucidate the nature of PDRM lock-in processes in marine sediments. However, mechanisms such as microbial activity, changes in sediment composition, and particle (flocculation) sizes, changes in chemical conditions, etc., are likely to be relevant. Overall, further efforts with similar and additional approaches are needed to better understand PDRM lock-in.

7. Conclusions

Quantitative model studies have addressed the PDRM acquisition process in marine sediments and reveal that filtering of the geomagnetic signal will occur during PDRM lock-in. However, details of the filter function and the thickness of the PDRM lock-in zone remain topics of debate. We have performed forward and inverse model calculations to estimate the best-fit filter function and thickness of the PDRM lock-in zone in marine sediments based on comparison between ^{10}Be flux and relative paleointensity records. A time-dependent eddy diffusion model was used to represent vertical biological mixing and was determined from the stratigraphic dispersion of microtektites. Forward modeling results indicate that a Gaussian function with a 17 cm lock-in zone thickness is the most suitable for representing the PDRM lock-in process for the available data. Filtering with other functions (linear, exponential, and cubic) appears to overly smooth the input signal. An empirical PDRM lock-in function obtained by inverse modeling also reveals that PDRM lock-in intensifies in the middle of the lock-in zone, contrary to expectations from other functions. This likely explains why PDRM lock-in is delayed relative to other sedimentary records, while filtering of the geomagnetic signal remains relatively small. Our results also suggest that the PDRM is not simply locked as a result of progressive consolidation and dewatering of marine sediments, and that commonly used lock-in functions that are used to model PDRM lock-in starting from the base of the surface mixed layer may not be appropriate for explaining the observed paleomagnetic signal in marine sediments.

Acknowledgments

We thank Hirokuni Oda for suggestions concerning microtektite analysis. Chris Grimshaw and Kerry Swanson assisted with microscopic analysis at the University of Canterbury, New Zealand. We also are grateful for the constructive comments of the Editor, Peter deMenocal, and four anonymous referees. This work was partially supported by JSPS Kakenhi (21253001, 21674003, 20300294, 00344614, and NEXT program GR031), the Sumitomo Foundation (093491), and a Sasakawa Scientific Research Grant (JSS-21-334). The production of this paper was supported by an NIPR publication subsidy.

Appendix

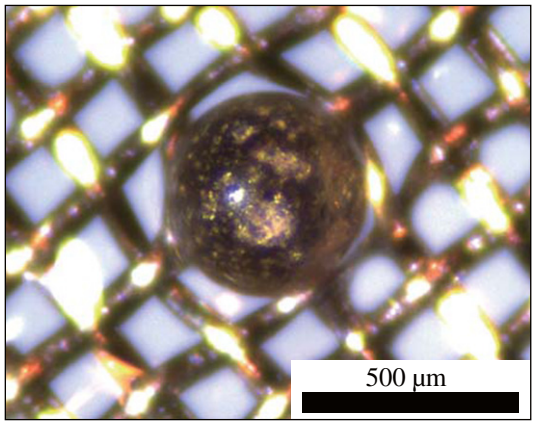

Fig. A.1. Photograph of a microtektite from core MD982187 at a depth of 12.86 m as seen under a stereomicroscope.

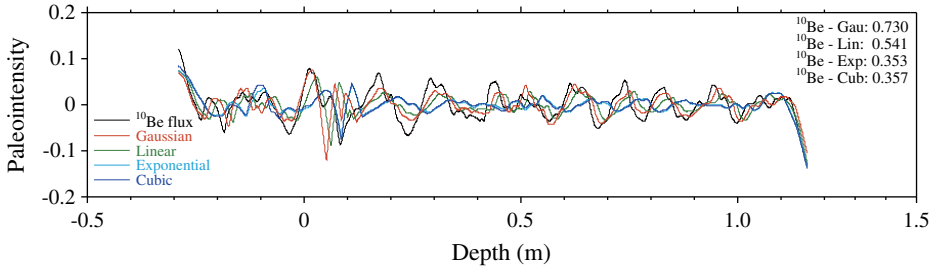

Fig. A.2. High-pass filtered ^{10}Be flux and paleointensity records for each lock-in function (Gaussian, linear, exponential, and cubic). A Butterworth type high-pass filter with a cut-off frequency of 0.006 cycle/mm was used for this analysis. The correlation coefficients between the calculated ^{10}Be and all paleointensity records are listed on the figure.

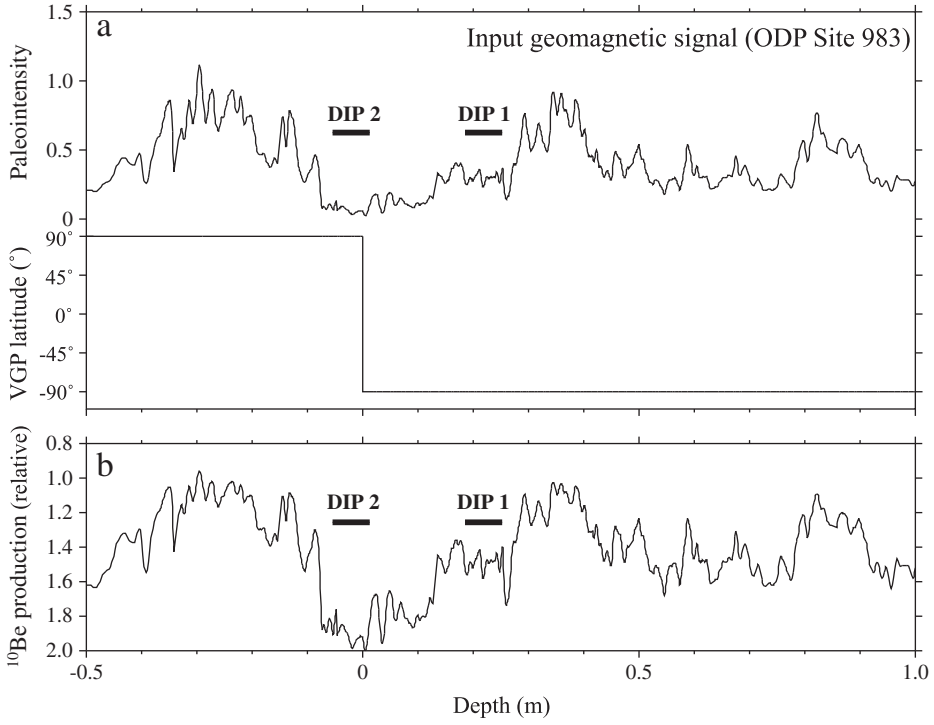

Fig. A.3. Paleointensities, VGP latitudes, and ^{10}Be flux record employed as the input geomagnetic signal for forward modeling. (a) The input geomagnetic signal is transferred from the paleomagnetic record of Channell and Kleiven (2000) from ODP Site 983 onto an artificial depth scale based on the average sedimentation rate of the Brunhes Chron (1.65 cm) for core MD982187. The geomagnetic polarity change in this model is simplified to a single instantaneous switch in VGP latitude. A depth of 0 m is assigned to the M–B boundary. (b) ^{10}Be flux record calculated using the relative paleointensity record in (a) based on the relationship for ^{10}Be production with respect to geomagnetic field intensity from Wagner et al. (2000).

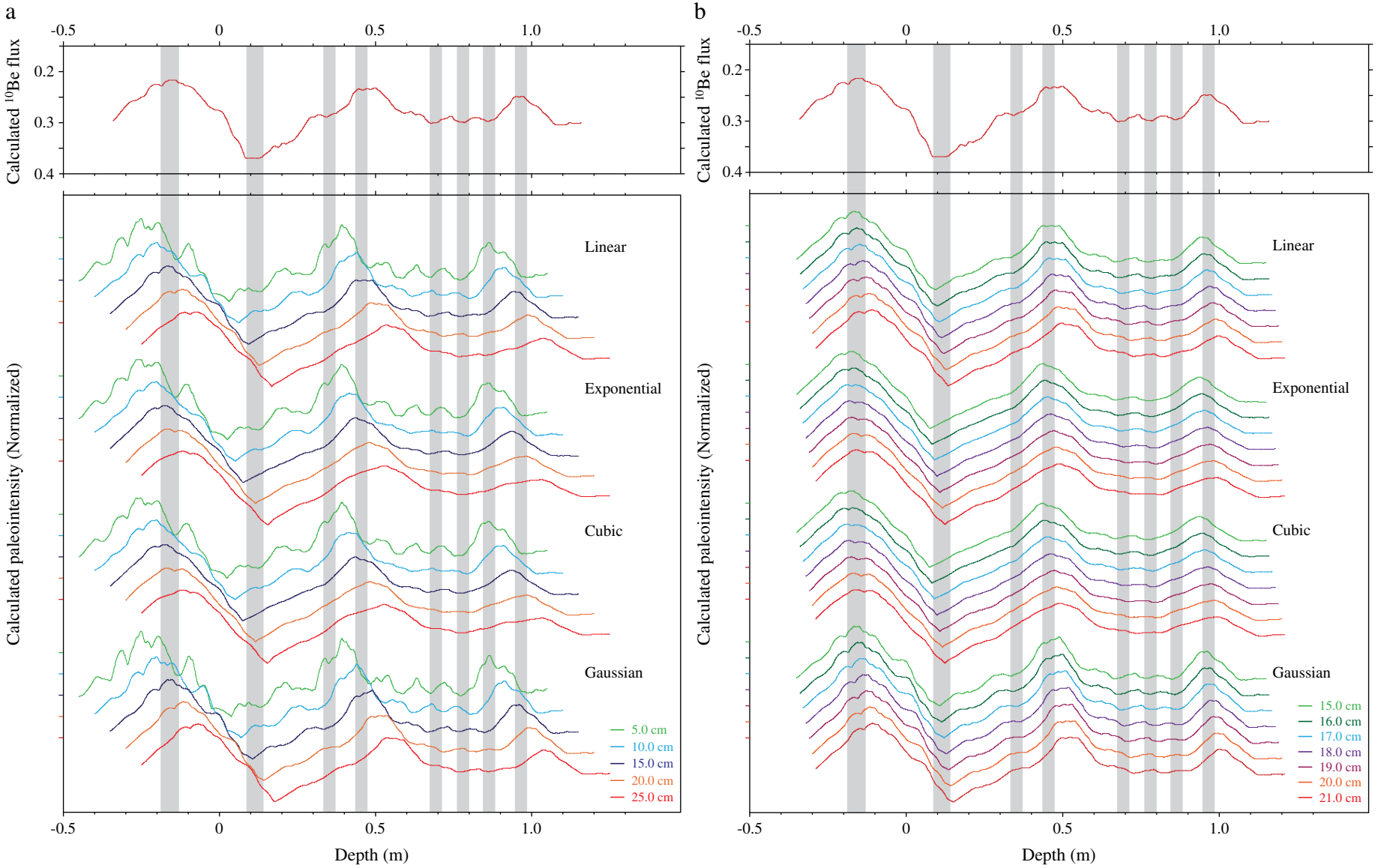

Fig. A.4. Paleointensity records calculated using linear, exponential, cubic, and Gaussian functions for lock-in zones with *F* values of (a) 5, 10, 15, 20, and 25 cm, and (b) 15, 16, 17, 18, 19, 20, and 21 cm. A simple VGP change (single instantaneous switch in VGP latitude) is used as an input signal for this calculation. Upper panel: ^{10}Be flux calculated using a mixing function to represent bioturbation (gray shading: ^{10}Be flux maxima and minima).

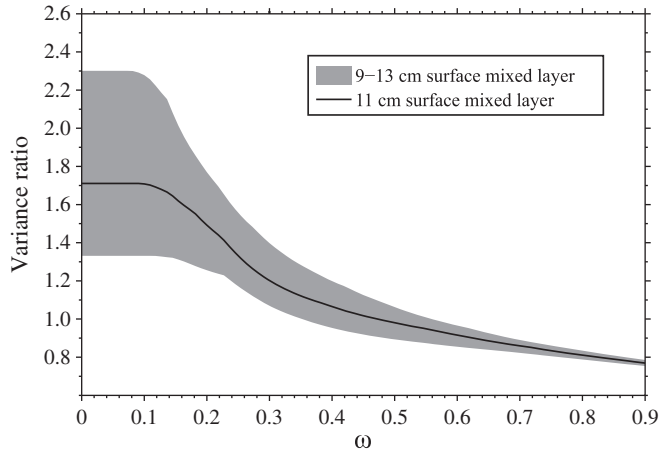

Fig. A.5. Illustration of the water level regularization scheme employed to limit noise amplification during deconvolution. The scheme yields smoother deconvolved ^{10}Be flux records as the threshold parameter, ω, is increased. To assess the level of smoothing, the ratio of the variance of the deconvolved ^{10}Be flux record is compared to the variance of the measured sedimentary record of ^{10}Be flux. In cases where the variance ratio is <1, the deconvolved ^{10}Be flux has a lower variance than the sedimentary record, which does not fit accepted ideas concerning smoothing due to bioturbation. As shown by the shaded region, the variance ratio also depends on the assumed thickness of the surface mixed layer.

Table A.1
Distribution of microtektites (>125 μm) from core MD982187.

Depth (m)	Count/100 mg
12.79	0
12.82	0
12.83	3
12.84	0
12.85	0
12.86	7
12.87	7
12.89	10
12.91	13
12.92	7
12.93	7
12.94	20
12.96	0
12.97	0
12.99	0
13.01	0
13.04	0

Table A.2
Correlation coefficients between calculated paleointensity and ^{10}Be flux records for different lock-in zone thicknesses. A simple VGP change (single instantaneous switch in the VGP latitude) is used as an input signal for the calculation.

Thickness of lock-in zone	Function			
	Linear	Exponential	Cubic	Gaussian
5	0.550	0.527	0.526	0.565
10	0.794	0.751	0.750	0.818
15	0.963	0.929	0.928	0.970
16	0.977	0.951	0.950	**0.975**
17	**0.979**	0.964	0.964	0.967
18	0.972	0.972	0.971	0.948
19	0.960	**0.974**	**0.973**	0.922
20	0.942	0.971	0.971	0.891
21	0.920	0.965	0.965	0.855
25	0.797	0.907	0.908	0.677

Bold indicates optimal correlation.

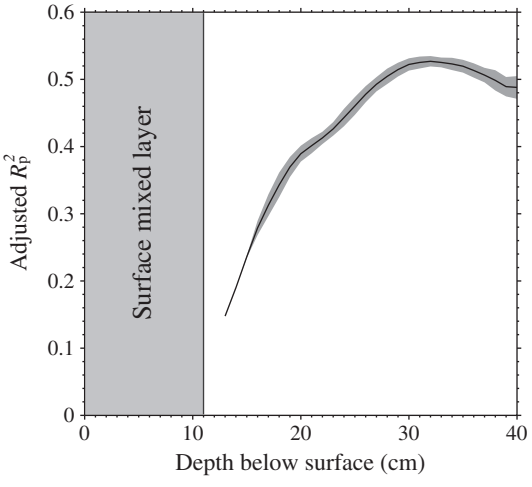

Fig. A.6. Illustration of the model selection procedure used to determine the best-fit inverse model. The first 11 cm of the lock-in function corresponds to the surface mixed layer (shaded) and it is assumed that no lock-in occurs within this zone. With increasing thickness, the value of R^2_p increases and reaches a maximum at 32 cm. As lock-in zone thickness increases, R^2_p decreases, which indicates that improvement in the model fit by increasing the width of the lock-in function is insufficient to compensate for the increase in the number of degrees of freedom. The shading around the black line represents the standard deviation on R^2_p estimated from 100 runs of the optimization algorithm with different initializations.

References

Aster, R.C., Borchers, B., Thurber, C., 2005. Parameter Estimation and Inverse Problems. Elsevier Academic Press, New York.

Bleil, U., von Dobeneck, T., 1999. Geomagnetic events and relative paleointensity records—clues to high-resolution paleomagnetic chronostratigraphies of Late Quaternary marine sediments? In: Fischer, G., Wefer, G. (Eds.), Use of Proxies in Paleoceanography: Examples from the South Atlantic. Springer-Verlag, Berlin, Heidelberg, pp. 635–654.

Boudreau, B.P., 1994. Is burial velocity a master parameter for bioturbation? Geochim. Cosmochim. Acta 58, 1243–1249.

Boudreau, B.P., 1998. Mean mixed depth of sediments: the wherefore and the why. Limnol. Oceanogr. 43, 524–526.

Carter-Stiglitz, B., Valet, J.P., LeGoff, M., 2006. Constraints on the acquisition of remanent magnetization in fine-grained sediments imposed by redeposition experiments. Earth Planet. Sci. Lett. 245, 427–437.

Channell, J.E.T., Guyodo, Y., 2004. The Matuyama Chronozone at ODP Site 982 (Rockall Bank): evidence for decimeter-scale magnetization lock-in depths. AGU Geophys. Monogr. Ser. 145, 205–219.

Channell, J.E.T., Kleiven, H.F., 2000. Geomagnetic palaeointensities and astrochronological ages for the Matuyama–Brunhes boundary and the boundaries of the Jaramillo Subchron: palaeomagnetic and oxygen isotope records from ODP Site 983. Philos. Trans. R. Soc. London, Ser. A 358, 1027–1047.

deMenocal, P.B., Ruddiman, W.F., Kent, D.V., 1990. Depth of post-depositional remanence acquisition in deep-sea sediments — a case-study of the Brunhes–Matuyama reversal and oxygen isotopic stage-19.1. Earth Planet. Sci. Lett. 99, 1–13.

Gradstein, F.M., Ogg, J.G., Smith, A., (eds), 2004. A Geologic Time Scale 2004. Cambridge University Press.

Guinasso Jr., N.L., Schink, D.R., 1975. Quantitative estimates of biological mixing rates in abyssal sediments. J. Geophys. Res. 80, 3032–3043.

Hamano, Y., 1980. An experiment on the post-depositional remanent magnetization in artificial and natural sediments. Earth Planet. Sci. Lett. 51, 221–232.

Hartl, P., Tauxe, L., 1996. A precursor to the Matuyama/Brunhes transition-field instability as recorded in pelagic sediments. Earth Planet. Sci. Lett. 138, 121–135.

Horng, C.S., Roberts, A.P., Liang, W.T., 2003. A 2.14-Myr astronomically tuned record of relative geomagnetic paleointensity from the western Philippine Sea. J. Geophys. Res. 108, 2059. doi:10.1029/2001JB001698.

Hyodo, M., 1984. Possibility of reconstruction of the past geomagnetic-field from homogeneous sediments. J. Geomagn. Geoelec. 36, 45–62.
Ikehara, K., Nishimura, A., 1993. Physical property of sediments along the 20° N transect from Hawaii to Mariana and in the West Caroline Basin, 1992FY report on "Marine Geological Study on Element Cycles in Ocean". Geol. Surv. Jpn. 67–74.
Ikehara, K., Nishimura, A., Kawahata, H., Iizasa, K., 1992. Physical property of sediments from the Philippine Sea and West Caroline Basin, 1991FY report on "Marine Geological Study on Element Cycles in Ocean". Geol. Surv. Jpn. 134–164.
Inoue, S., Yamazaki, T., 2010. Geomagnetic relative paleointensity chronostratigraphy of sediment cores from the Okhotsk Sea. Palaeogeogr. Palaeoclimatol. Palaeoecol. 291, 253–266.
Irving, E., Major, A., 1964. Post-depositional detrital remanent magnetization in a synthetic sediment. Sedimentology 3, 135–143.
Katari, K., Tauxe, L., 2000. Effects of pH and salinity on the intensity of magnetization in redeposited sediments. Earth Planet. Sci. Lett. 181, 489–496.
Kent, D.V., 1973. Post-depositional remanent magnetisation in deep sea sediment. Nature 246, 32–34.
Kent, D.V., Schneider, D.A., 1995. Correlation of paleointensity variation records in the Brunhes/Matuyama polarity transition interval. Earth Planet. Sci. Lett. 129, 135–144.
Kiefer, T., Sarnthein, M., Erlenkeuser, H., Grootes, P.M., Roberts, A.P., 2001. North Pacific response to millennial-scale changes in ocean circulation over the last 60 kyr. Paleoceanography 16, 179–189.
Knudsen, M.F., Henderson, G.M., Frank, M., MacNiocaill, C., Kubik, P.W., 2008. In-phase anomalies in Beryllium-10 production and palaeomagnetic field behaviour during the Iceland Basin geomagnetic excursion. Earth Planet. Sci. Lett. 265, 588–599.
Lagarias, J.C., Reeds, J.A., Wright, M.H., Wright, P.E., 1998. Convergence properties of the Nelder–Mead simplex method in low dimensions. SIAM J. Optim. 9, 112–147.
Laj, C., Kissel, C., Mazaud, A., Channell, J.E.T., Beer, J., 2000. North Atlantic palaeointensity stack since 75 ka (NAPIS-75) and the duration of the Laschamp event. Philos. Trans. R. Soc. London, Ser. A 358, 1009–1025.
Lal, D., Peters, B., 1967. Cosmic ray produced radioactivity on the Earth. In: Fluegge, S., Sitte, K. (Eds.), Handbuch der Physik. Springer-Verlag, Berlin, pp. 551–612.
Lambe, T.W., Whitman, R.V., 1969. Soil Mechanics. John Wiley, New York.
Liu, Q.S., Roberts, A.P., Rohling, E.J., Zhu, R.X., Sun, Y.B., 2008. Post-depositional remanent magnetization lock-in and the location of the Matuyama–Brunhes geomagnetic reversal boundary in marine and Chinese loess sequences. Earth Planet. Sci. Lett. 275, 102–110.
Macri, P., Sagnotti, L., Dinarès-Turell, J., Caburlotto, A., 2010. Relative geomagnetic paleointensity of the Brunhes Chron and the Matuyama–Brunhes precursor as recorded in sediment core from Wilkes Land Basin (Antarctica). Phys. Earth Planet. Inter. 179, 72–86.
Mazaud, A., Sicre, M.A., Ezat, U., Pichon, J.J., Duprat, J., Laj, C., Kissel, C., Beaufort, L., Michel, E., Turon, J.L., 2002. Geomagnetic-assisted stratigraphy and sea surface temperature changes in core MD94-103 (Southern Indian Ocean): possible implications for North–South climatic relationships around H4. Earth Planet. Sci. Lett. 201, 159–170.
Meynadier, L., Valet, J.P., 1996. Post-depositional realignment of magnetic grains and asymmetrical saw-tooth patterns of magnetization intensity. Earth Planet. Sci. Lett. 140, 123–132.
Officer, C.B., Lynch, D.R., 1983. Determination of mixing parameters from tracer distributions in deep-sea sediment cores. Mar. Geol. 52, 59–74.
Otofuji, Y., Sasajima, S., 1981. A magnetization process of sediments: laboratory experiments on post-depositional remanent magnetization. Geophys. J. R. Astron. Soc. 66, 241–259.
Roberts, A.P., Winklhofer, M., 2004. Why are geomagnetic excursions not always recorded in sediments? Constraints from post-depositional remanent magnetization lock-in modeling. Earth Planet. Sci. Lett. 227, 345–359.
Sagnotti, L., Budillon, F., Dinarès-Turell, J., Iorio, M., Macri, P., 2005. Evidence for a variable paleomagnetic lock-in depth in the Holocene sequence from the Salerno Gulf (Italy): implications for "high-resolution" paleomagnetic dating. Geochem. Geophys. Geosyst. 6, Q11013. doi:10.1029/2005GC001043.
Schneider, D.A., Kent, D.V., Mello, G.A., 1992. A detailed chronology of the Australasian impact event, the Brunhes–Matuyama geomagnetic polarity reversal, and global climate change. Earth Planet. Sci. Lett. 111, 395–405.
Singer, B.S., Hoffman, K.A., Coe, R.S., Brown, L.L., Jicha, B.R., Pringle, M.S., Chauvin, A., 2005. Structural and temporal requirements for geomagnetic field reversal deduced from lava flows. Nature 434, 633–636.
Stoner, J.S., Channell, J.E.T., Hillaire-Marcel, C., Kissel, C., 2000. Geomagnetic paleointensity and environmental record from Labrador Sea core MD95-2024: global marine sediment and ice core chronostratigraphy for the last 110 kyr. Earth Planet. Sci. Lett. 183, 161–177.
Stott, L., Poulsen, C., Lund, S., Thunell, R., 2002. Super ENSO and global climate oscillations at millennial time scales. Science 297, 222–226.
Suganuma, Y., Yamazaki, T., Kanamatsu, T., 2009. South Asian monsoon variability during the past 800 kyr revealed by rock magnetic proxies. Quat. Sci. Rev. 28, 926–938.
Suganuma, Y., Yokoyama, Y., Yamazaki, T., Kawamura, K., Horng, C.S., Matsuzaki, H., 2010. ^{10}Be evidence for delayed acquisition of remanent magnetization in marine sediments: implication for a new age for the Matuyama–Brunhes boundary. Earth Planet. Sci. Lett. 296, 443–450.
Swan, A.R.H., Sandilands, M., 1995. Introduction to Geological Data Analysis. Blackwell Press, Oxford.
Tauxe, L., Yamazaki, T., 2007. Paleointensities. In: Kono, M. (Ed.), Treatise on Geophysics: Geomagnetism, 5. Elsevier, New York, pp. 509–563.
Tauxe, L., Herbert, T., Shackleton, N.J., Kok, Y.S., 1996. Astronomical calibration of the Matuyama–Brunhes boundary: consequences for magnetic remanence acquisition in marine carbonates and the Asian loess sequences. Earth Planet. Sci. Lett. 140, 133–146.
Tauxe, L., Steindorf, J.L., Harris, A., 2006. Depositional remanent magnetization: toward an improved theoretical and experimental foundation. Earth Planet. Sci. Lett. 244, 515–529.
Thomson, J., Brown, L., Nixon, S., Cook, G.T., MacKenzie, A.B., 2000. Bioturbation and Holocene sediment accumulation fluxes in the north-east Atlantic Ocean (Benthic Boundary Layer experiment sites). Mar. Geol. 169, 21–39.
Valet, J.P., Meynadier, L., 1993. Geomagnetic field intensity and reversals during the past four million years. Nature 366, 234–238.
Valet, J.P., Meynadier, L., Guyodo, Y., 2005. Geomagnetic dipole strength and reversal rate over the past two million years. Nature 435, 802–805.
Verosub, K.L., 1977. Depositional and post-depositional processes in the magnetization of sediments. Rev. Geophys. Space Phys. 15, 129–143.
Wagner, G., Masarik, J., Beer, J., Baumgartner, S., Imboden, D., Kubik, P.W., Synal, H.A., Suter, M., 2000. Reconstruction of the geomagnetic field between 20 and 60 kyr BP from cosmogenic radionuclides in the GRIP ice core. Nucl. Instrum. Methods Phys. Res., Sect. B 172, 597–604.
Yamazaki, T., 1992. Water content of surface sediments in the south of the Nova-Canton Trough, Central Equatorial Pacific (GH82-4 AREA): relevance to acquisition of depositional remanent magnetization. Geol. Surv. Jpn. Cruise Rep. 22, 127–133.
Yamazaki, T., Oda, H., 2005. A geomagnetic paleointensity stack between 0.8 and 3.0 Ma from equatorial Pacific sediment cores. Geochem. Geophys. Geosyst. 6, Q11H20. doi:10.1029/2005GC001001.